An Acad Bras Cienc (2022) 94(2): e20210678 DOI 10.1590/0001-3765202220210678
Anais da Academia Brasileira de Ciências | *Annals of the Brazilian Academy of Sciences*
Printed ISSN 0001-3765 I Online ISSN 1678-2690
www.scielo.br/aabc | www.fb.com/aabcjournal

GEOSCIENCES

Some features of solitonic waves propagating in intermediate waters

LUIZ GALLISA GUIMARÃES

Abstract: This work addresses the problem of weakly non linear ocean waves propagation in intermediate waters. We have shown that the propagation of waves similar to hole solitons, as well as progressive waves of high intensity multipeaks are likely to occur in this non linear regime. In addition, we note that along intermediate waters, these particular non-linear waves satisfy a wave equation model similar to Korteweg de Vries equation, and their propagation features strongly depend on the initial conditions adopted to the present problem.

Key words: ocean waves, extreme waves, non linear waves, solitons in fluids, hydrodynamics.

INTRODUCTION

Since the beginning of our early civilizations, the waves propagating in the ocean or even reaching the coast, have always fascinated the human imagination, whether by the feelings of beauty and fear that evoke us. From these ancient times to nowadays, human economic and cultural activities have always expanded and developed across the ocean, especially trade between peoples and countries, and today a large part of global economic activity involves navigation. Therefore, the study of nature (Lighthill 1978, Dean & Dalrymple 1991), generation (Holthuijsen 2010, Svendsen 2006), propagation (Dingemans 1997, Babanin 2011) and wave forecasting models (Osborne 2010, Campos et al. 2018, 2019) in the ocean has long been an active area of interdisciplinary research. Waves are potentially dangerous, their impact can be tremendously devastating, causing the destruction and disruption of human activities in coastal areas (Holthuijsen 2010, Svendsen 2006), as well as damaging and even sinking ships in the deep ocean (Kharif et al. 2008). On the other hand, it is known that the greater the height of the wave, the greater the energy it carries (Lighthill 1978, Dean & Dalrymple 1991, Holthuijsen 2010). In addition, nonlinear effects can amplify the height of the wave in both shallow and deep waters (Dean & Dalrymple 1991, Dingemans 1997, Osborne 2010). In this work we will be interested in understanding how some of these nonlinear effects occur when the wave propagates in intermediate waters. More specifically, we will study some characteristics of solitary waves (or simply, solitons) propagating in intermediate waters (Remoissenet 1999, Drazin & Johnson 1989). To this end, we will outline this article as follows, in the next section for pedagogical reasons, we will make a quick review of the main concepts involving linear wave propagation in finite depth oceans, as well as in the subsequent section, we use these concepts to introduce an alternative approach to analyze the problem of wave propagation in intermediate waters. Keeping these ideas in mind, in the later

sections we will obtain a new non-linear differential equation that governs the propagation of waves in intermediate waters, and we will show also that this differential equation allows hole solitons (Chabchoub et al. 2012, 2014) as one of its solutions, being the behavior of these solitons extremely sensitive to the initial conditions proposed for this particular problem (Chabchoub et al. 2012, 2014, Kibler et al. 2015). Finally, in the last section we will comment and summarize our main results.

MATERIALS AND METHODS

Harmonic waves in intermediate waters

In this section we will review some fundamental features related to harmonic progressive waves propagation in oceans with finite depth d and impenetrable seabed. Under these conditions, it is well known that for a given period T, local gravity g and wavelength $\lambda(T,d)$, these harmonic waves should satisfy the following dispersion relationship (Lighthill 1978, Dean & Dalrymple 1991):

$$\omega = \sqrt{g\ k\ \tanh(kd)}. \tag{1}$$

Where $\omega = 2\pi/T$ being the circular frequency, while $k = 2\pi/\lambda$ is the wavenumber. Furthermore, solving this dispersion relationship (1) for $k(\omega,d)$, it is possible to obtain the phase $c = \omega/k$ and group $u = \partial\omega/\partial k$ wave velocities, which are respectively related to spatial wavefront displacement and the energy flow through the ocean. More explicitly we have c and u given by (Lighthill 1978, Dean & Dalrymple 1991),

$$c = \sqrt{\frac{g}{k}\tanh(kd)} \tag{2}$$

and

$$u = \frac{c}{2}\left[1 + \frac{2kd}{\sinh(2kd)}\right]. \tag{3}$$

In addition, for harmonic waves $\eta(x,t) = A\sin(k[x-ct])$ propagating in the horizontal x–direction, the horizontal velocity υ of the particles at given depth z is written as (Holthuijsen 2010):

$$\upsilon(x,z,t) = c\ \frac{kA\cosh[k(z+d)]\sin(kx-\omega t)}{\sinh(kd)}. \tag{4}$$

Being A the wave amplitude and it assumed that the linear approximation for waves with small amplitudes is hold (Dean & Dalrymple 1991). Continuing our analysis on oceanic wave propagation and in order to gain some more physical insight about this problem, it is suitable to rewrite the dispersion relationship (1) as a function of the period T and wavelength λ, namely (Svendsen 2006):

$$\lambda(T,d) = \frac{g\ T^2}{2\pi}\tanh\left[\frac{2\pi\ d}{\lambda(T,d)}\right]. \tag{5}$$

Moreover, it is interesting to note that the above transcendental equation(5) has an explicit solution for the wavelength $\lambda(T,d)$ in both asymptotic limits related to shallow and deep waters (Dean & Dalrymple 1991, Lighthill 1978). For instance, in the first case associated with shallow water, in such a way that it occurs at the limit where the depth $d \mapsto 0$, follows that Eq.(5) solutions $\lambda \mapsto \lambda_0$ (Dean & Dalrymple 1991, Lighthill 1978) are given by,

$$\lambda_0(T,d) = T\ \sqrt{g\ d}. \tag{6}$$

On the other hand in the shallow water limit, we can observe from Eqs.(2 and 3) that the phase c_0 and group u_0 velocities behave as,

$$c_0(d) \approx \sqrt{gd} \approx u_0(d). \tag{7}$$

This last result suggests a low dispersion of wave packets in this propagation regime. However, as in this limit the phase velocity c_0 varies with the variation of the depth d, it is expected that these waves strongly refract during their propagation in shallow waters (Dean & Dalrymple 1991). In addition, it is important to note that some physical features of the wave propagation in deep waters are quite different from those in shallow waters. In other words, at the limit of great depths where $d \mapsto \infty$ (Dean & Dalrymple 1991, Lighthill 1978), the solution of the transcendental equation (5) shows that the wavelengths are given by,

$$\lambda \mapsto \lambda_\infty(T) = c_\infty T, \tag{8}$$

where in this situation the wave phase velocity c_∞ behaves as,

$$c_\infty(T) = gT/2\pi = 2 \times u_\infty(T). \tag{9}$$

The above equation (9) shows that in deep waters the value of the phase velocity c_∞ is twice the group velocity u_∞, this fact suggests that in this case there is a strong dispersion of wave packets (Dean & Dalrymple 1991, Lighthill 1978), as well as showing that the during the wave propagation its direction should not vary substantially, since both c_∞ and u_∞ are only wave period T functions.

In general, there are in the literature (Dean & Dalrymple 1991, Lighthill 1978) more explicit numerical criteria quantifying shallow and deep water limits. These criteria are related to the asymptotic behavior of "$\tanh(2\pi\delta)$" function as the value of the ratio $\delta \equiv d/\lambda$ varies. For instance, based on particular mathematical accuracy criteria, the literature suggests that the shallow water limit $\delta \equiv \delta_0$ is reached when $\delta_0 = 0.05$ (according to Dean & Dalrymple 1991), as well as the value $\delta_0 = 0.07$ can also be accepted (this last one was adopted by Lighthill 1978). On the other hand, in the other extreme case of deep water where $\delta \equiv \delta_\infty$, it is usual to adopt the numerical accuracy criteria as $\delta_\infty = 0.50$ (Dean & Dalrymple 1991) or $\delta_\infty = 0.28$ (Lighthill 1978). In addition, it is assumed that the wave is propagating in intermediate waters when a specific ratio δ_i is within the range $\delta_0 < \delta_i < \delta_\infty$. For example, (Lighthill 1978) adopts $\delta_i \approx 0.16$ as a typical value for waves propagation on intermediate waters. Besides, in order to gain a little more physical insights into these issues, as well as strongly based on many ideas discussed in Lighthill's seminal textbook about waves in fluids (Lighthill 1978, Chapter 3, pp. 218, Fig. 53), here as an initial assumption, we assume that the wave are in intermediate waters when the depth $d \equiv d_i$ is such that, $\lambda_0(T, d_i) \approx \lambda_\infty(T)$ or equivalently $c_0(T, d_i) \approx c_\infty(T)$. For instance, see panels a) and b) in Fig. (1) where we exemplify these results for a wave period $T = 5$s. In general under these above assumptions, for waves with a given period T and comparing Eqs. (6 and 8), we can adopt that the intermediate depth d_i behaves as,

$$d_i(T) = \frac{\lambda_\infty(T)}{2\pi} = \frac{g}{\omega^2}\,. \tag{10}$$

Moreover, the above equation (10) allows us to rewrite the transcendental equation (5) in the following suitable dimensionless form,

$$[\lambda\,/\lambda_\infty] = \tanh\left(\frac{h}{[\lambda\,/\lambda_\infty]}\right). \tag{11}$$

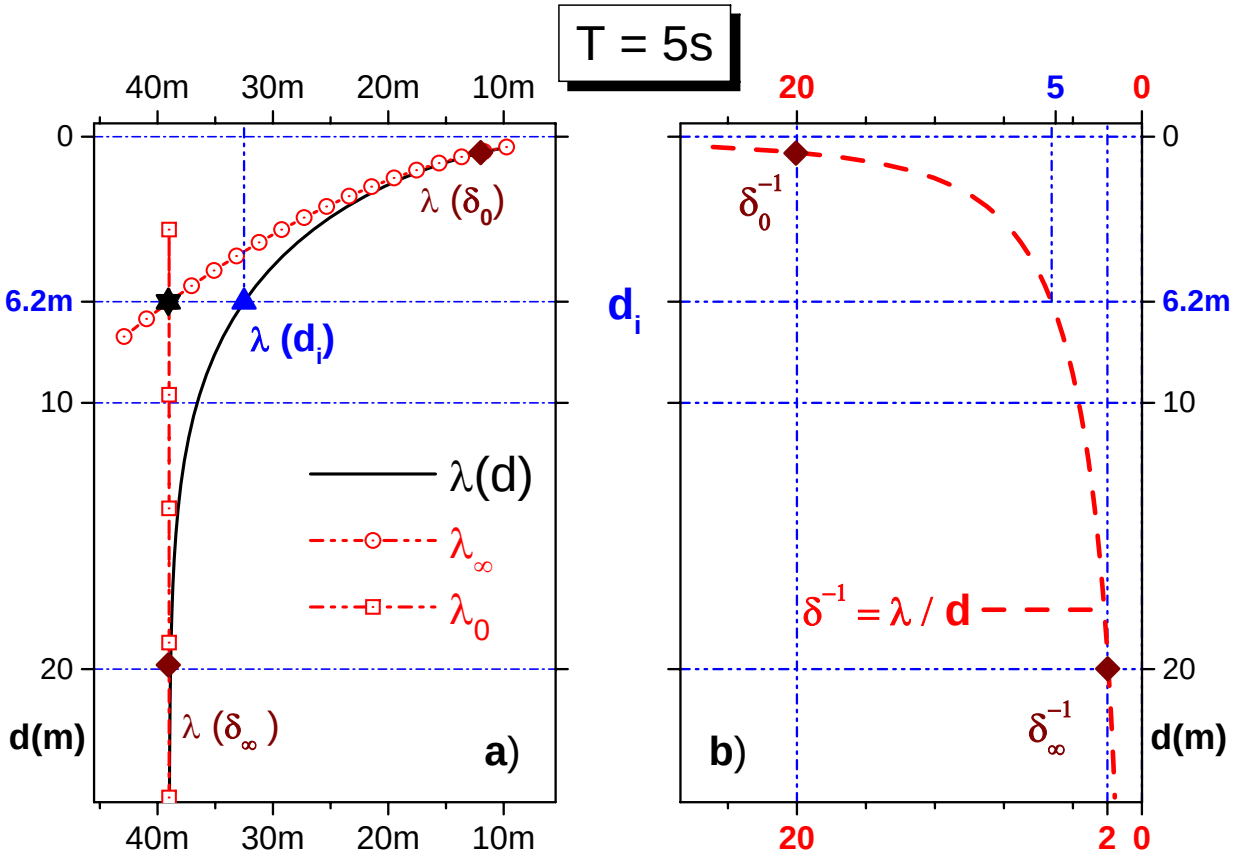

Figure 1. for a wave with period $T = 5$s, the panel a) shows the behavior of the wavelengths λ and λ_0 as a function of the depth d and the deep water wavelength λ_∞. It is also noted that $\lambda_0 = \lambda_\infty$ at depth d_i. The panel b) shows that in shallow waters $\lambda/d_i \approx 5$ is limited between δ_0^{-1} and δ_∞^{-1}, these results are in accordance with those pioneering discussed in (Lighthill 1978).

Where we define the dimensionless depth scale h as,

$$h(T,d) \equiv \frac{d}{d_i(T)}. \tag{12}$$

In addition, in the present problem the Snell's wave refraction law is hold and it means that the wave should undergo a change in the wavefront propagation direction as its phase velocity $c(T,d) \leq c_\infty(T)$ varies (Dean & Dalrymple 1991), more explicitly for a given period T and depth d we have to,

$$\frac{\sin(\theta(T,d))}{c(T,d)} = \frac{1}{c_\infty(T)} = cte, \tag{13}$$

where the refraction angle θ indicates the change in wavefront propagation direction from its initial path in deep water. On the other hand, as $\lambda(T,d) = c(T,d)T$, we can also rewrite the Snell law(13) in terms of wavelength,

$$\lambda(T,d) = \lambda_\infty(T)\sin(\theta(T,d)). \tag{14}$$

Using the latter result(14) it is possible to explicitly solve equation (11) in terms of h as a function of the refraction angle θ,

$$h(\theta) = \sin(\theta) \ln\left(\sqrt{\frac{1+\sin(\theta)}{1-\sin(\theta)}}\right), 0 \leq h < \infty;\ 0 \leq \theta < \frac{\pi}{2}, \tag{15}$$

as well as to calculate the ratio $\delta \equiv d/\lambda = h/\left(2\pi \sin(\theta)\right)$ for a given θ. On the other hand, notice that for a given normalized depth h and explicitly adopting $\sin\theta(h)$ as an unknown independent variable, the last equation (15) can be numerically inverted in terms of the refraction angle $\theta(h)$. Details about this numerical procedure are given in Appendix A. Thereafter, it is opportune to continue our analysis assuming that the refraction angle $\theta(h)$ is known. In this way, follows of the Eqs. (3, 13 and 15) that in this new picture we can rewrite the phase c and group u velocities respectively as,

$$c(T,\theta) = c_\infty(T)\sin(\theta) \tag{16}$$

and,

$$u(T,\theta) = u_\infty(T)\left[\sin(\theta) + \cos(\theta)^2 \ln\left(\sqrt{\frac{1+\sin(\theta)}{1-\sin(\theta)}}\right)\right]. \tag{17}$$

Besides based on Eq. (17), it is interesting to note that the group velocity reaches a maximum value $u \equiv u_{max}$ as the angle of refraction reaches $\theta = \theta_m$, where u_{max} and $\sin(\theta_m)$ satisfy the following equations respectively,

$$u_{max}(T,\theta_m) = \frac{u_\infty(T)}{\sin(\theta_m)} \tag{18}$$

and

$$\ln\left(\frac{1+\sin(\theta_m)}{1-\sin(\theta_m)}\right) = \frac{2}{\sin(\theta_m)}. \tag{19}$$

Thus, comparing the above Eq. (19) with Eq. (15), we have that,

$$h(\theta_m) = h_i = 1. \tag{20}$$

More specifically, it is important to notice that for wave packets coming from deep waters up to depth $d = d_i(T)$, their group velocity reaches at the intermediate depth $d_i(T)$ a maximum value around $u_{max}(T,\theta_m) \approx 1.2u_\infty(T)$ (see Fig. 2b). Thus, we can give the physical meaning to *the intermediate depth d_i as the depth at which the wave packets have their maximum group velocity value u_{max}*, this value being around 20% greater than the initial group velocity value in deep waters u_∞. Besides, Eqs. (10, 12 and 20) suggest that in this situation, it is possible to assume that the depth d_i can be adopted as a typical depth for waves with period T propagating in the intermediate waters. In parallel, the panels a) and b) in Fig. (2) show that both wave phenomena, dispersion and refraction play a relevant role in the propagation of waves in intermediate waters. More specifically at the intermediate depth d_i (see Fig. 2b), where the wave packet reaches its maximum group velocity value u_{max}. From Eq. (20) and Fig. (2a), it is observed that at the depth d_i the refraction angle reaches the following value:

$$\theta(h_i) = \theta_m \approx \arcsin\left(0.83356\right). \tag{21}$$

Therefore it is deduced from the above estimate (21) (see Eqs. 71 and 72 for more numerical details) that the wave in its course from its generation in deep ocean, until reaching intermediate waters with

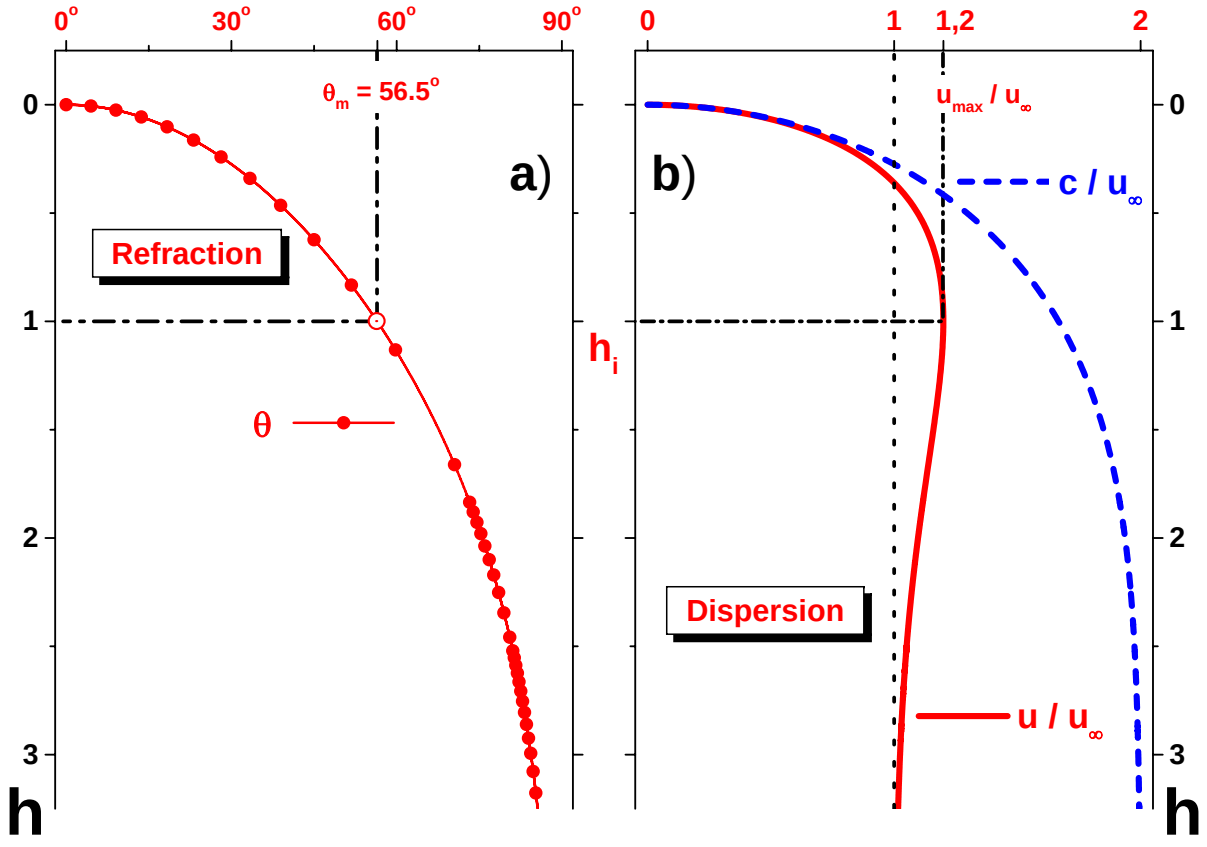

Figure 2. shows in panel a) the wave refraction angle θ as a function of the dimensionless depth h. The panel b) shows the behavior of the phase c and group u velocities as h varies. Note that u reaches a maximum value u_{max} at $h_i \equiv 1$, and that around these intermediate waters ($d \approx d_i$) the wave refractive and dispersive effects are still very significant.

depths close to the value d_i, such wave performs an arc of $\theta_m \approx 5\pi/16 \approx 56.5^o$. Moreover for depths values around $d \approx d_i$, it also follows from the estimate(21) and Eqs. (16 and 17), that wave packets propagating in intermediate waters are still quite dispersive, since the ratio between their phase and group velocities behaves as:

$$\frac{u_{max}(T,\theta_m)}{c(T,\theta_m)} = \frac{1}{2\sin(\theta_m)^2} \approx 0.72. \tag{22}$$

In addition, although in intermediate waters the interactions of the waves with the seabed are not very intense, it is possible that refraction and dispersion of the waves combined with non-linear effects may already smoothly alter the shape of the wave. In other words, here we assume that due to the energy of wave refraction and dispersion, or even soft interaction of the waves with the seabed generating weak nonlinear effects, the shape and the slope of waves may vary during their propagation in intermediate waters (Dean & Dalrymple 1991, Holthuijsen 2010, Svendsen 2006, Dingemans 1997). In this way, it is plausible that these effects may be related to changes in the horizontal component of underwater particles velocity. Thus, in order to characterize these changes, we will calculate during the half-period $T/2$, the mean variation $\Delta\upsilon$ between the horizontal velocity components for particles that are located

at $z = -A$ close to the wave trough, and those that are close to the wave crest at the depth $z = +A$. Using Eq. (4) we obtain that,

$$\begin{aligned}\Delta\upsilon(x,t,k,d) &\equiv [\upsilon(x,A,t) - \upsilon(x,-A,t+T/2)]/2 \\ &= c\frac{\cosh(kA)}{\tanh(kd)}\, k\, A \sin(kx - \omega t) \\ &\approx \frac{c}{\tanh(kd)}\, k\, \eta + O(A^3)\,. \end{aligned} \tag{23}$$

Where we have assumed that in intermediate waters the assumption of wave simple shoaling is hold (Svendsen 2006) and the amplitude A behaves as,

$$A \approx A_\infty \sqrt{u_\infty / u}, \tag{24}$$

being A_∞ the wave amplitude in deep waters. Besides, due to the ratio u_∞/u, Eqs. (24 and 23) suggest that wave dispersion plays a fundamental role in wave shoaling even in intermediate waters and for $u = u_{max}$, the Eqs. (24 and 20) show that the wave amplitude A reaches at $h_i = 1$ the minimum value $A_{min} \approx 0.9 A_\infty$.

Natural Boundaries for Intermediate Waters

Complementing the results discussed above, our next step is to characterize the frontiers between shallow and intermediate waters as well as the natural boundaries between deep and intermediate waters. To this end, based on the pioneering works (Jogesh Babu et al. 2002, Kakizawa 2004, Bremnes 2019) we will adopt here a similar picture in which we will characterize the possibility of occurrence of any undulatory physical phenomena such as wave refraction, dispersion and shoaling as a possible "random" process occurring at a given normalized depth h. In addition, we assume that it is feasible to associate a *cross correlation continuous density function* (**CCCDF**) to these processes as h varies. More specifically, here as first approximation, we make the roughly assumption that we can associate any wave propagation phenomenon listed above with a CCCDF, just by relating this to a single Bernstein polynomial B with degree two (Jogesh Babu et al. 2002, Kakizawa 2004, Bremnes 2019), namely:

$$B[\Theta(h)] = b\,\Theta(h)\,[1 - \Theta(h)] \quad ;\; 0 \le \Theta(h) \le 1 \quad ,\forall\, 0 \le h < \infty, \tag{25}$$

where b is an arbitrary normalization constant such that,

$$b \equiv \left[\int_0^\infty dh \;\; \Theta^2 (1-\Theta)^2\right]^{-1/2}. \tag{26}$$

In addition, for a given h the function $\Theta(h)$ should describe the successful occurrence possibility of a specific wave phenomenon at the normalized depth h, while the term $[1 - \Theta(h)]$ is the chance of the opposite situation where such phenomenon does not occur. In this binomial probabilistic framework, it is important to analyze the behavior of the derivative of B as h varies, where in the present case the derivative $B' \equiv \partial B/\partial h$ is given by,

$$B'[\Theta(h)] = -2b\left(\Theta(h) - \frac{1}{2}\right)\frac{\partial\Theta(h)}{\partial h}. \tag{27}$$

On the other hand, for some particular dimensionless depths h_*, we notice from above Eqs. (27 and 25) that B can reach its maximum or minimum values in the following cases where $\Theta(h_*) = 1/2$ or $\Theta'(h_*) = 0$. In other words, here we assume h_* as a possible natural depth scale related to some specific wave phenomenon associated with the behavior of the function $\Theta(h)$ (or $1 - \Theta(h)$), considering that these natural phenomena have maximum or minimum occurrence chance at the depth h_*. In order to clarify and illustrate these concepts for some usual ocean undulatory phenomena, we show in Fig. (3) for such cases the behavior of B and its derivative B' as the depth h varies. More specifically, in this figure we relate the wave phenomena refraction, dispersion and refraction–dispersion with the followings suitable $\Theta(h)$ functions, namely:

$$\Theta_R \equiv \sin(\theta) \quad \left(0 \leq \theta < \frac{\pi}{2}\right), \tag{28}$$

$$\Theta_D \equiv \frac{\Delta v_\infty}{\Delta v}, \tag{29}$$

and

$$\Theta_{RD} \equiv \Theta_R \times \Theta_D . \tag{30}$$

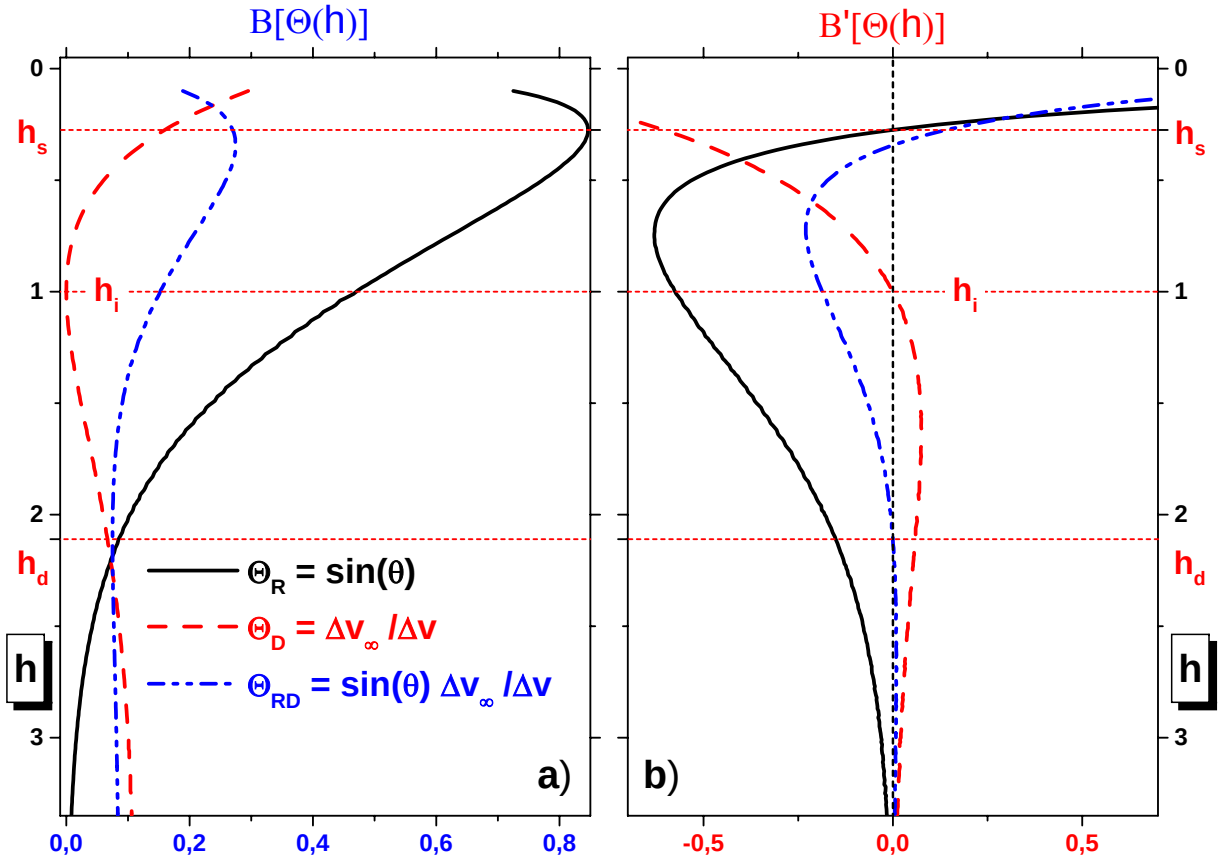

Figure 3. sketches the behavior of the CCCDF, in the cases associated with refraction and dispersion of waves as well as for the situation where the refraction and dispersion effects can occur simultaneously. Note that the panels a) and b) show respectively how in these cases the Bersntein's polynomial B and its derivative B' behave as h varies.

In this way, both panels in Fig. (3) suggest that adopting the criterion discussed above, where the points of maximum or minimum values of Bersntein polynomials(25) are the most probabilistically relevant points (see Eq. 27), we see for example that in shallow waters Θ_R reaches a maximum value in $h_s = \ln(3)/4 \approx 0.275$. In parallel, we can also notice from both panels in Fig. (3) that in the case of intermediate waters, Θ_D reaches a minimum in $h_i = 1$. Finally, we can associate the beginning of the transition between intermediate and deep waters in $h_d = 2.11$, since Θ_{RD} reaches a minimum at this depth. Moreover, in the present framework using the above results and applying the Eqs. (71 and 72), we can estimate that when the wave leaves deep waters and penetrates into intermediate waters, its wave front has been refracted at an angle of about $\theta(h_d) \equiv \theta_d \approx 77^o$. On the other hand, using again the same procedure we can note that when the wave is leaving intermediate waters and beginning its propagation in shallow waters, we can calculate the refraction angle of the wave as $\theta(h_s) \equiv \theta_s = 30^o$. Besides, in order to compare the present picture based on Bersntein polynomials(25) schema with well established criteria (Dean & Dalrymple 1991, Lighthill 1978), we notice that using Eq. (15) we can conclude that the ratio δ between depth d and wavelength λ, reaches in shallow, intermediate and deep waters the following values, $\delta(h_s) \equiv \delta_s \approx 0.087$, $\delta(h_i) \equiv \delta_i \approx 0.191$ and $\delta(h_d) \equiv \delta_d \approx 0.345$ respectively (see Table I).

Table I. based on CCCDF summarizes the limits between the regions here established as normalized shallow depth $h_s \approx 0.275$, intermediate depth at $h_i = 1$ and deep waters a part from $h_d \approx 2.11$ respectively. Besides, it is also shown the ratio $\delta = d/\lambda$ and the refraction angle θ related to these waters.

h_*	$\delta(h_*)$	$\theta(h_*)$
h_s	$\delta_s \approx 0.087$	$\theta_s = 30.0^o$
h_i	$\delta_i \approx 0.191$	$\theta_m \approx 56.5^o$
h_d	$\delta_d \approx 0.345$	$\theta_d \approx 77.0^o$

These above results are in accordance with those reported in Refs. (Dean & Dalrymple 1991, Lighthill 1978, Holthuijsen 2010, Svendsen 2006). It is also worth mentioning that from now on, we will restrict our analysis to particular situations on waves propagating in intermediate waters. More specifically, we will study only some wave propagation cases where the depth h varies between $h_s \leq h \leq h_d$. Using semi-classical physics arguments, we will discuss in the next section the features of weak non linear waves propagating in such intermediate waters regions.

SOLITONIC WAVE PROPAGATION IN INTERMEDIATE WATERS

In the case of oceanic waves, it is well known that during their propagation, the shape and the skewness of the wave changes (Dean & Dalrymple 1991, Lighthill 1978, Holthuijsen 2010, Svendsen 2006). To better understand these wave transformations in intermediate waters, we think that it is suitable to adopt a reference frame that moves with the average velocity $\Delta\upsilon$ (see Eq. 23), since $\Delta\upsilon$ represents *the magnitude of the velocities of particles located between the wave trough and crest*, and

certainly these wave extreme points are sensitive to changes during the wave shoaling process. On the other hand, to begin this analysis we will use the analogy of this problem with those related to wave propagation in presence of currents and flows (Dean & Dalrymple 1991, Holthuijsen 2010, Remoissenet 1999, Milewski & Keller 1996, Milewski 2005). In this way, we assume that in this particular referential frame (Remoissenet 1999, Sec.5.5), the dispersion relationship (1) can be now approximated by,

$$\omega - k\,\Delta\upsilon \approx \sqrt{g\,k\,\tanh\left(k\,\left[d+\,\eta\right]\right)}\,. \tag{31}$$

Assuming again the small amplitude approximation (see Eq. 23), we can rewrite Eq. (31) in the following suitable form,

$$\omega\sqrt{\frac{d}{g}} \approx P\left(kd\right) + \eta\;k\,Q\left(kd\right)\;. \tag{32}$$

Where the functions P and Q are given respectively by,

$$P\left(kd\right) \equiv \sqrt{kd\tanh\left(kd\right)}, \tag{33}$$

and

$$Q\left(kd\right) \equiv \frac{\sqrt{kd\tanh\left(kd\right)}\;\left[\sinh\left(2\,kd\right)+\tanh\left(kd\right)\right]^{-1}}{\sqrt{\tanh\left(kd\right)+\,\mathrm{sech}\left(kd\right)^{2}\;\ln\left[\left(1+\tanh\left(kd\right)\right)/\mathrm{sech}\left(kd\right)\right]}} \tag{34}$$

On the other hand, before we discuss about some wave propagation features related to the dispersion relationship (32), we think it is pedagogically useful to analyze the asymptotic limits of both ultra-deep and ultra-shallow water. More specifically, it is interesting to note that at these extreme depth limits $d \mapsto \infty$ or $d \mapsto 0$, Eq. (32) permits us respectively obtain the following asymptotic behaviour of the phase velocity $\widetilde{c}$ related to such waves, namely:

$$\widetilde{c}_{\infty} \approx c_{\infty}\left(1+2\,k\,\eta\right)\;, \tag{35}$$

and

$$\widetilde{c}_{0} \approx c_{0}\left[1-\frac{\left(kd\right)^{2}}{6}\;+\frac{3\sqrt{2}}{4\sqrt{kd}}\,\frac{\eta}{A_{\infty}}\right]\;. \tag{36}$$

It is interesting to notice that Eq. (35) resembles the phase velocity of Stokes waves propagating in ultra deep water (Remoissenet 1999, Drazin & Johnson 1989). On the other hand, Eq. (36) differs from those related to the phase velocity of nonlinear waves derived from Korteweg–de Vries(KdV) wave like equations (Remoissenet 1999, Drazin & Johnson 1989). More specifically, in the present asymptotic model for wave propagation in ultra shallow water, such competition between nonlinearity and wave dispersion is no longer related to the Ursell number (Remoissenet 1999), but rather to the expression $\left[9\sqrt{2}\;\eta\;/\;\left(2\left(kd\right)^{5/2}A_{\infty}\right)\right]$, that is the ratio between the asymptotic leading terms in Eq. (36). In other words, this latter fact suggests that waves that satisfy the dispersion relationship (32), when propagating in shallow water, should behave differently from those that are solutions of the usual KdV wave equation. Hereafter, we will discuss in more detail the propagation of these nonlinear waves in intermediate waters. For this purpose, it is important take into account that in the present geometrical framework we can write $kd = h/\sin(\theta)$, and in order to apply semi-classical methods to this problem for waves in intermediate waters, we notice that it is suitable to expand both functions P and Q in kd

powers (Remoissenet 1999, Drazin & Johnson 1989, Dingemans 1997). On the other hand, rather than adopting a methodology for studying the behavior of the above dispersion relationship (32) based on Padé–Taylor expansions *around some specific depth* (Remoissenet 1999, Drazin & Johnson 1989, Dingemans 1997), we will here choose to adopt an analysis that can be *accurately satisfactory for any depth over the full range of intermediate waters*. More specifically, for convenience we choose for this task, $\forall h$ with $h_s \leq h \leq h_d$, the *Chebyshev* polynomial basis (Arfken & Weber 1999, Press et al. 2007), where based on symmetry issues[1], we obtain the following explicit expansions in kd monomials odd powers respectively,

$$P(kd) \mapsto P_T(kd) = L_1 kd + L_3 (kd)^3 + L_5 (kd)^5 , \tag{37}$$

and

$$Q(kd) \mapsto Q_T(kd) = N_1 kd + N_3 (kd)^3 . \tag{38}$$

Being L_n and N_n, respectively, the coefficients of the P_T and Q_T Chebyshev polynomials above. Such coefficients are listed in Table II. We note from Fig. (4a) that expansion(37) is completely held along the intermediate waters, but Fig. (4b) suggests that approximation(38) is not well accurate in regions around very shallow waters for depths h close to h_s.

Table II. shows the numerical values of the coefficients L_n and N_n related to the Chebyshev polynomials P_T and Q_T expansions respectively.

n	L_n	N_n
1	22660/24111	32381/27242
3	-7741/100000	5827/98707
5	53/12500	

On the other hand, in analogy with Non Linear Schrödinger equations framework theories (Remoissenet 1999, Dingemans 1997, Drazin & Johnson 1989, Osborne 2010), here we will adopt respectively the following normalized dimensionless horizontal length ξ and time τ scales, namely:

$$\xi \equiv \frac{x}{d_i} \tag{39}$$

and

$$\tau \equiv 2\pi \frac{t}{T} . \tag{40}$$

Moreover adopting this procedure, it is possible to rewrite the usual *semi-classical mapping* $k \mapsto -i\,\partial/\partial x$ and $\omega \mapsto i\,\partial/\partial t$ (Remoissenet 1999, Dingemans 1997, Schiff 1955), in the following suitable form,

$$d\,k \mapsto -i\,h\,\frac{\partial}{\partial \xi} \tag{41}$$

and

$$\sqrt{\frac{d}{g}}\,\omega \mapsto i\,\sqrt{h}\,\frac{\partial}{\partial \tau} . \tag{42}$$

[1]In this preliminary analysis, dissipative effects are not taken into account and we assume the ocean surface as a medium where the $T - P$ symmetries (temporal reversion and spatial inversion) must be preserved (Schiff 1955).

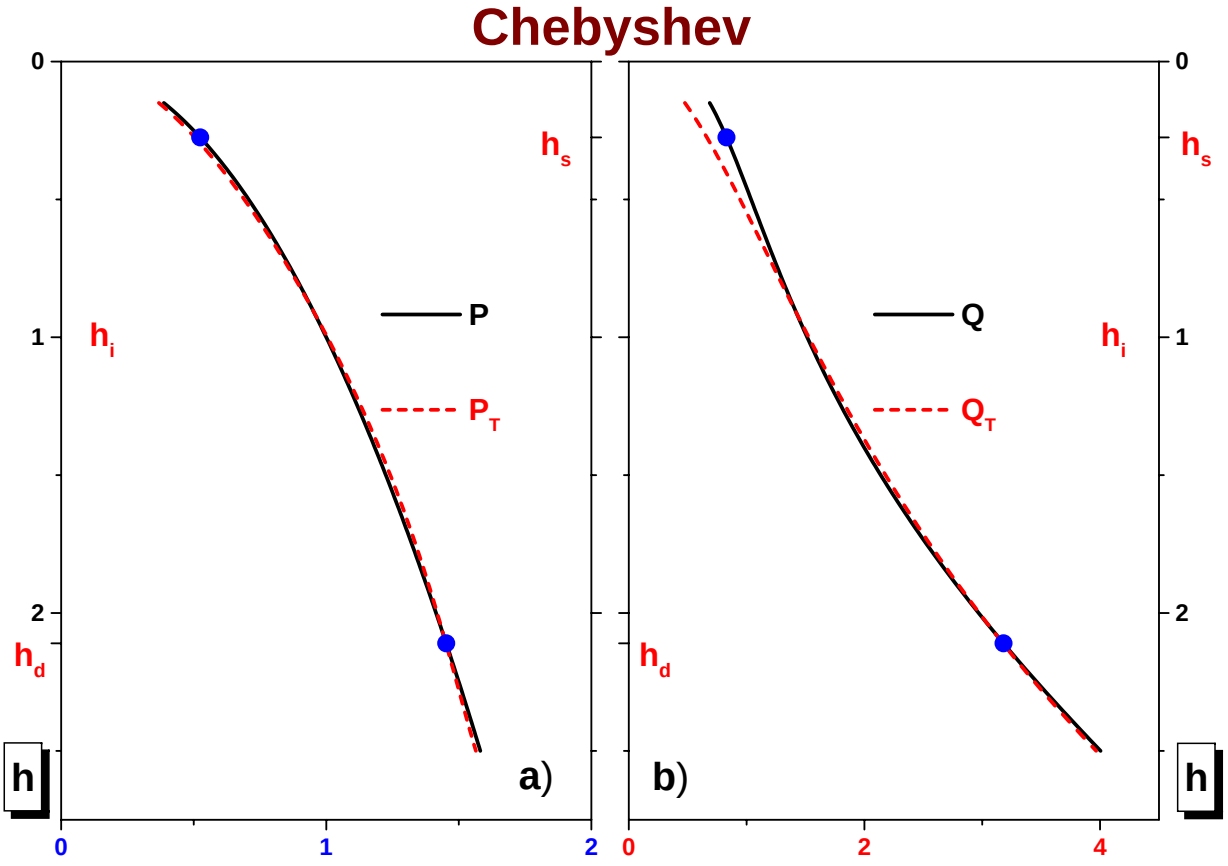

Figure 4. compares in panels a) and b) the expansions in Chebychev polynomials P_T and Q_T for the functions P and Q respectively. Note in a) that P_T fits P well in the whole range $h_s \leq h \leq h_d$, while the panel b) shows that Q_T also fits Q well for depths in deep and intermediate waters, but the difference between Q_T and Q increases around shallow waters. In both panels, the full dots delimit the range between deep and shallow waters $h_s \leq h \leq h_d$.

Thus applying the above semi-classical maps(41 and 42) into the Chebyshev polynomial approximations (37 and 38), we can map the dispersion relationship (32) in a KdV like equation (Remoissenet 1999, Dingemans 1997, Drazin & Johnson 1989), being this procedure hold for waves in intermediate waters where $h_s \leq h \leq h_d$. More specifically, in this framework we obtain that the waveforms $\eta(x,t) \mapsto W(\xi,\tau)$ should satisfy the following non linear partial differential equation, namely:

$$\mathcal{L} + \aleph = 0\,. \tag{43}$$

Where the linear $\mathcal{L}$ and non linear $\aleph$ terms of the above differential partial equation (43) are given respectively by,

$$\begin{aligned}\mathcal{L} = &\frac{\partial}{\partial\xi}W(\xi,\tau) + \frac{1}{L_1\sqrt{h}}\frac{\partial}{\partial\tau}W(\xi,\tau)\\ &-\frac{L_3h^2}{L_1}\frac{\partial^3}{\partial\xi^3}W(\xi,\tau) + \frac{L_5h^4}{L_1}\frac{\partial^5}{\partial\xi^5}W(\xi,\tau)\end{aligned} \tag{44}$$

and

$$\aleph = W(\xi,\tau)\left(\frac{N_1}{L_1 h}\frac{\partial}{\partial\xi}W(\xi,\tau) - \frac{N_3 h}{L_1}\frac{\partial^3}{\partial\xi^3}W(\xi,\tau)\right) . \tag{45}$$

On the other hand, using the simple and powerful method developed by Jawad (2013), it is possible to obtain an explicit and analytic $W(\xi,\tau) = W(\kappa\,\xi - \nu\,\tau)$ waveform solutions of the above non-linear partial differential equation (43). More specifically, here we find that these particular solutions can behave as solitons, namely:

$$W(\kappa\,\xi - \nu\,\tau) = a_0 + a_2\,[\mathrm{sech}\,(\kappa\,\xi - \nu\,\tau)]^2 . \tag{46}$$

Where, for any above particular solution $W(\kappa\xi - \nu\,\tau)$, with complex arbitrary dimensionless wavenumber $\kappa = \Re[\kappa] + i\,\Im[\kappa] \in \mathbb{C}$, the coefficients a_0, a_2 and the dimensionless frequency parameter ν should satisfy the following equations respectively,

$$a_0(h,\kappa) = \frac{h}{2{N_3}^2}\left(20\,\kappa^2\,h^2\,L_5N_3 + 5\,L_5N_1 - 2\,L_3N_3\right) , \tag{47}$$

$$a_2(h,\kappa) = -30\,\kappa^2\,h^3\,\frac{L_5}{N_3} , \tag{48}$$

and

$$\nu(h,\kappa) = -\frac{\kappa}{2}\sqrt{h}\left(48\,\kappa^4h^4L_5 - 5\,\frac{L_5{N_1}^2}{{N_3}^2} + 2\,\frac{N_1L_3}{N_3} - 2\,L_1\right) . \tag{49}$$

In order to analyze in more details the behavior of the above waveform solution $W(\Phi)$, it is important to notice that since $\kappa \in \mathbb{C}$, the wave function W argument

$$\begin{aligned}\Phi &\equiv \kappa\xi - \nu\,\tau \\ &\equiv X + i\,Y\end{aligned} \tag{50}$$

is a complex function either, where its real and imaginary parts are written respectively as,

$$\begin{aligned}X(\xi,\tau,h,\kappa) &\equiv \Re(\Phi) \\ &= \xi\,\Re(\kappa) - \tau\,\Re(\nu(h,\kappa))\end{aligned} \tag{51}$$

and

$$\begin{aligned}Y(\xi,\tau,h,\kappa) &\equiv \Im(\Phi) \\ &= \xi\,\Im(\kappa) - \tau\,\Im(\nu(h,\kappa)) .\end{aligned} \tag{52}$$

Thus, follows of the above Eqs. (51 and 52) that the real and imaginary parts of the function $\mathrm{sech}\,(\Phi)^2$ are respectively given by,

$$\Re\left[\mathrm{sech}\,(\Phi)^2\right] = \frac{[\mathrm{sech}\,(X)\sec(Y)]^2\left(1 - [\tanh(X)\tan(Y)]^2\right)}{\left(1 + [\tanh(X)\ \tan(Y)]^2\right)} \tag{53}$$

and

$$\Im\left[\mathrm{sech}\,(\Phi)^2\right] = -2\frac{\tanh(X)\tan(Y)\,[\mathrm{sech}\,(X)\sec(Y)]^2}{\left(1 + [\tanh(X)\ \tan(Y)]^2\right)} . \tag{54}$$

The above Eqs. (53 and 54) suggest that the general solution (46) is a wave train modulated by hyperbolic functions, where the phase velocities $U_{\Re}$ of modulating and $U_{\Im}$ related to carrier waves (see Eqs. 51 and Eqs. 52) should respectively satisfy the following equations:

$$U_{\Re} = \frac{\Re(\nu)}{\Re(\kappa)}\, c_{\infty}\ ;\ \forall\, \Re(\kappa) \neq 0 \tag{55}$$

and

$$U_{\Im} = \frac{\Im(\nu)}{\Im(\kappa)}\, c_{\infty}\ ;\ \forall\, \Im(\kappa) \neq 0\,. \tag{56}$$

More specifically, we see that Eq. (46) allows the existence of finite modulating waves such as "sech^2" like as well as spatially extended "tanh" like solutions. On the other hand, based on the poles behavior of the oscillating functions tan(Y) and sec(Y), we notice in Eqs. (53 and 54) that along the wave propagation path, these carrier waves can present discrete caustics like singularities. It occurs for some particular points along the wave trajectory $(\xi_{\ell}, \tau_{\ell})$ that satisfy the following criteria,

$$\xi_{\ell} - \frac{U_{\Im}}{c_{\infty}}\, \tau_{\ell} = \pm\, \frac{\pi}{\Im(\kappa)} \left(\ell + \frac{1}{2}\right)\ ;\forall \Im(\kappa) \neq 0 \text{ and } \ell = 0, 1, 2, ... \tag{57}$$

On the other hand, different from the case of linear harmonic waves, Eq. (46) suggests that these solitonic waves have a non-zero mean level value. Furthermore, during the normalized time range $0 \leq \tau \leq 2\pi$ related to a single harmonic wave period T (see Eq. 40), it is possible to define for these waves(46) an initial mean level $\overline{W}$ in the following manner,

$$\begin{aligned}\overline{W}(\kappa\xi) &\equiv \frac{1}{2\pi}\int_0^{2\pi} d\tau\ W(\kappa\xi - \nu\ \tau) \\ &= a_0 + a_2\ \frac{\tanh(\kappa\xi) - \tanh(\kappa\xi - 2\,\nu\,\pi)}{2\nu\,\pi}\,.\end{aligned} \tag{58}$$

In general, depending on the κ and "tanh" function behaviors, the mean level $\overline{W}$ can also reach complex values as the depth h varies. In addition, in order to avoid some undesirable numerical instabilities and to be able to better clarify this initial analysis of the present problem, here we consider it useful to define the waveform mean relative level $\Delta\Omega$ as the following real function,

$$\Delta\Omega(\xi, \tau, \kappa) \equiv \Re\left(\frac{W - \overline{W}}{\overline{W}}\right) + \Im\left(\frac{W - \overline{W}}{\overline{W}}\right)\ ;\forall\, \overline{W} \neq 0. \tag{59}$$

NUMERICAL RESULTS

Thereafter, we will study some special features of these solitons propagating in intermediate waters. To this end, we have to point out that the dimensionless wavenumber $\kappa \in \mathbb{C}$ is a free parameter of this theory. So, we will examine in more detail some particular choices for κ that provide us with interesting scenarios for these solitonic waves W (see Eq. 46) propagation in intermediate waters. For instance, we now assume a particular wave propagation condition where the modulating wave phase velocity $U_{\Re}$ (see Eq. 55) has the same value of the single harmonic wave group velocity $u(h)$ (see Eq. 3). In other words, for any waveform W propagating in intermediate waters, we assume that the value of

its phase velocity is given by $U_{\Re} = u(h)$. This assumption allows us to obtain the following explicit equation for $\kappa(h)$:

$$\kappa(h) = \frac{\sqrt{3}}{6\,h}\left[6\left(\frac{5{N_1}^2}{2{N_3}^2} - \frac{N_1 L_3}{L_5 N_3} + \frac{L_1}{L_5}\right) - \frac{3}{L_5\sqrt{h}}\;\frac{u}{u_\infty}\right]^{\frac{1}{4}}. \tag{60}$$

Besides, follows of Eq. (49) that in this case the frequency ν varies with the depth h as,

$$\nu(h) = \frac{u\sqrt{3}}{12hu_\infty}\left[6\left(\frac{5{N_1}^2}{2{N_3}^2} - \frac{N_1 L_3}{L_5 N_3} + \frac{L_1}{L_5}\right) - \frac{3}{L_5\sqrt{h}}\frac{u}{u_\infty}\right]^{\frac{1}{4}}. \tag{61}$$

Then by using the data from Table II, we notice that in the above case, both $\kappa(h)$ and $\nu(h)$ are real positive functions for depths in intermediate waters satisfying $h_s \leq h \leq h_d$. In addition, for this case Fig. (5) shows the behavior of the waveform $\Delta\Omega$(see Eq. 59) in the $(\xi(h), \tau)$ plane as the depth h varies. More explicitly, the upper and lower panels of Fig. (5) show the behavior of $\Delta\Omega$ propagation along intermediate waters respectively in the scattered plot and level surfaces forms. In both panels in Fig. (5), it is interesting to note that in deep waters $\Delta\Omega$ behaves as a deeper trough similar to a kink, that when it propagates in shallow waters becomes a hole soliton that resembles internal waves in the ocean (Osborne 2010, Chap. 25). Finally, we note in both panels in Fig. (5) that this hole soliton waveform disappears in very shallow waters as the dimensionless horizontal propagation distance $\xi \to \infty$. It is also interesting to note that this curious behavior of $\Delta\Omega$(see Eq. 59) is partly due to the amplitude a_2 and the wave argument Φ softly vary during $\Delta\Omega$ propagation (see respectively Eqs. 48 and 50). In other words, in this particular case where κ satisfies Eq. (60), the variation in the initial form of $\Delta\Omega$ from a high water vacancy or very deep kink to a thin hole soliton in shallow water, it is in part associated with the fact that both $a_2(h)$ and $\Phi(h)$ are monotonic functions of depth h. This behavior can also be seen on the $\Delta\Omega$ amplitude grayscale map of Fig. (6), where the darker tonalities represent the deepest trough. It is also noted in Fig. 6 that for depths below $h \approx 1$, the changes in the form of $\Delta\Omega$ are more pronounced and that in very shallow waters as $h \to 0$ the hole soliton disappears.

We also study here another set of physical criteria about the propagation of these solitonic waves. These criteria revealed some very peculiar characteristics to this type of waves. More explicitly, if we admit that in a "distant past" the normalized wave strength has a given value S that satisfies,

$$\lim_{\tau \longrightarrow -\infty} W(\kappa\xi - \nu\,\tau) \equiv S\,, \tag{62}$$

and that in these case assuming in Eq. (46) that the term

$$\lim_{\tau \longrightarrow -\infty} \left[\operatorname{sech}(\kappa\xi - \nu\,\tau)\right]^2 \equiv 0\;\;, \tag{63}$$

can be also neglected, then it follows from Eq. (46) that κ must satisfy the following initial condition,

$$a_0(\kappa, h) = \;\; S\,. \tag{64}$$

Then follows of Eq. (47) that above equation (64) can be solved and the dimensionless wavenumber κ explicitly is given by:

$$\kappa(h, S) = \frac{\sqrt{10}}{10h\sqrt{h}}\sqrt{\frac{N_3}{L_5}\,S\; - \left(\frac{5N_1}{2\,N_3} - \frac{L_3}{L_5}\right)h}\,. \tag{65}$$

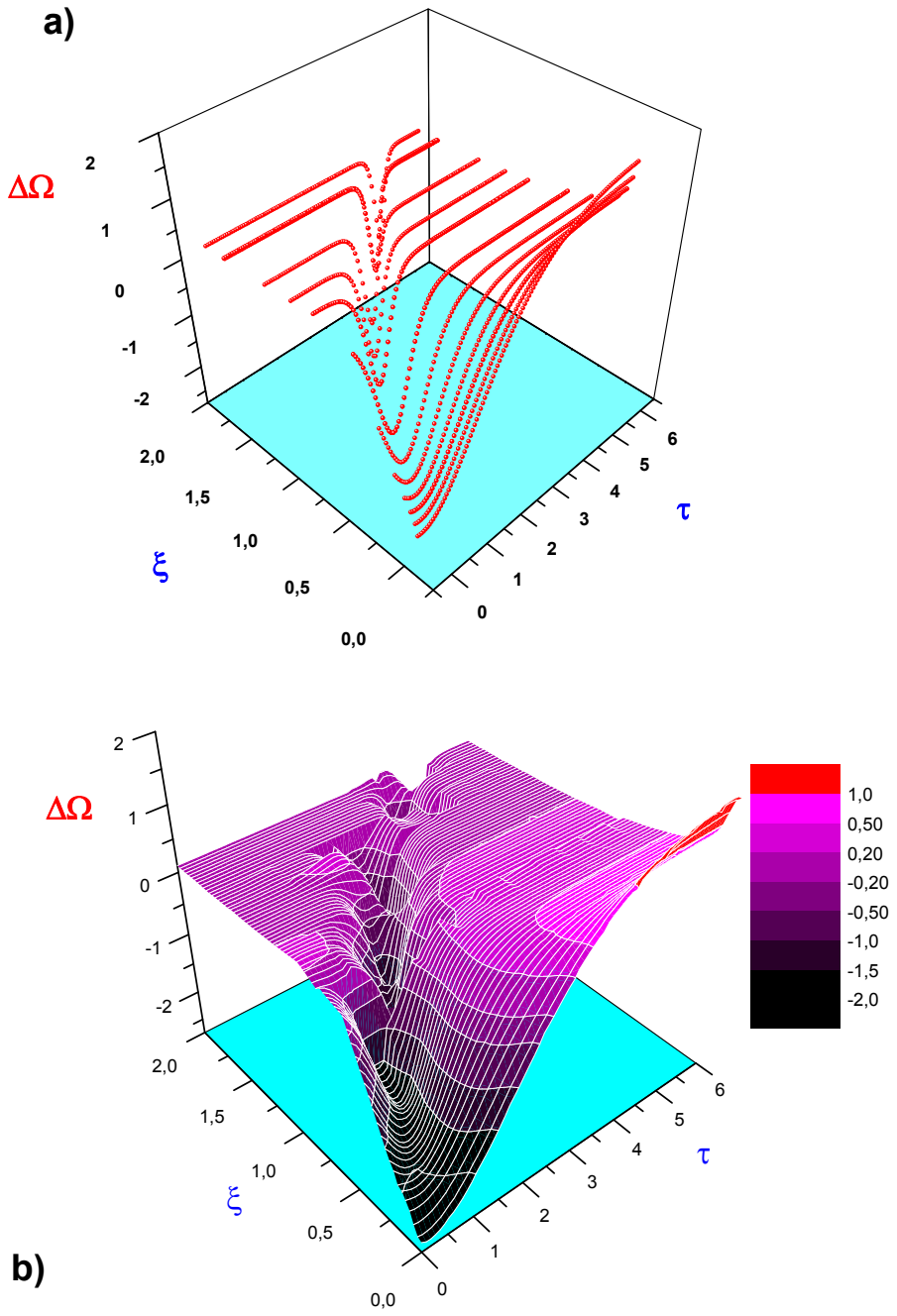

Figure 5. illustrates the propagation behavior of the $\Delta\Omega$ in the plane (ξ, τ). Both graphs, the first showing the scattered points in the panel (a) and the second related to the level surfaces represented in the panel (b), show that in deep waters ($\xi \approx 0$) the waveform $\Delta\Omega$ is a deeper trough (see color scale in bottom panel–b), and it becomes a hole soliton in intermediate waters ($\xi \approx 1$), but it cannot propagate in shallow waters as $\xi \to \infty$.

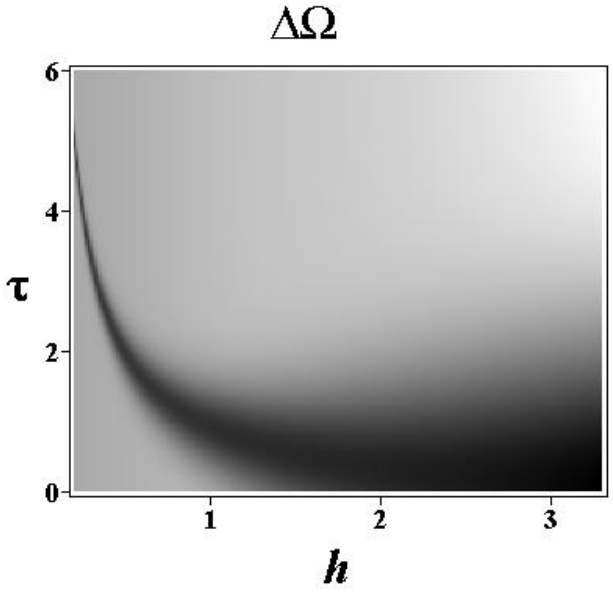

Figure 6. shows a grayscale map for the $\Delta\Omega$ normalized waveform behavior as the dimensionless time τ and depth h vary. In this map the widest and deepest water vacancies are represented by the darkest shades and they occur in large scale in deep waters ($h \gg h_d \approx 2.1$). It is also noted that in intermediate waters ($h \approx 1$), the hole soliton shape is well defined, and as this waveform reaches shallow water it becomes narrower and it disappears as $h \ll h_s \approx 0.28$.

Besides, follows of this Eq. (65) and Eq. (49) that in this particular situation the dimensionless frequency ν should satisfies the following equation,

$$\nu_S = \frac{\sqrt{10}}{10h^3}\sqrt{\frac{N_3}{L_5}\,S - \left(\frac{5N_1}{2\,N_3} - \frac{L_3}{L_5}\right)h} \times \left[\left(L_1 + \frac{N_1 L_3}{5N_3} + \frac{L_5 {N_1}^2}{{N_3}^2} - \frac{6{L_3}^2}{25L_5}\right)h^2 + \left(\frac{6N_1}{5} - \frac{12L_3N_3}{25L_5}\right)\,h\,S - \frac{6{N_3}^2}{25L_5}S^2\right] \tag{66}$$

Our next step is shown below, where depending on the value of S, this above solution can exhibit quite distinct behaviors for waveform propagation in intermediate waters (see Eq. 46). In this way, we will discuss in more detail the following particular initial wave propagation situations, the first in which S is related to the values of a wave trough, such as $S = -1$, as well as in another case, where the initial condition $S = 11$ being able to represent a wave crest, namely.

Case S = -1

In this particular situation such that $S = -1$, for any depth value in intermediate waters ($h_s \leq h \leq h_d$), the data in Table(II) show that the values of κ in Eq. (65) are purely imaginary complex numbers ($\Re(\kappa) = 0$ and $\Im(\kappa) \neq 0$). Therefore, it follows from Eq. (57) that it is possible that the waveform(46) can present extreme values during its propagation. This fact can be observed in both panels of Fig. (7), for example in the scatter plot panel(7a) we see in the plane (ξ, τ) some points with high $\Delta\Omega$ peak values. On the other hand, the level surface represented on the panel(7b) shows that the amplitude of these $\Delta\Omega$ peaks is intensified when the propagation distance assumes values around $x \approx d_i$, such that the normalized horizontal distance is close to $\xi \approx 1$ (see Eq. 39). On the other hand, it is possible

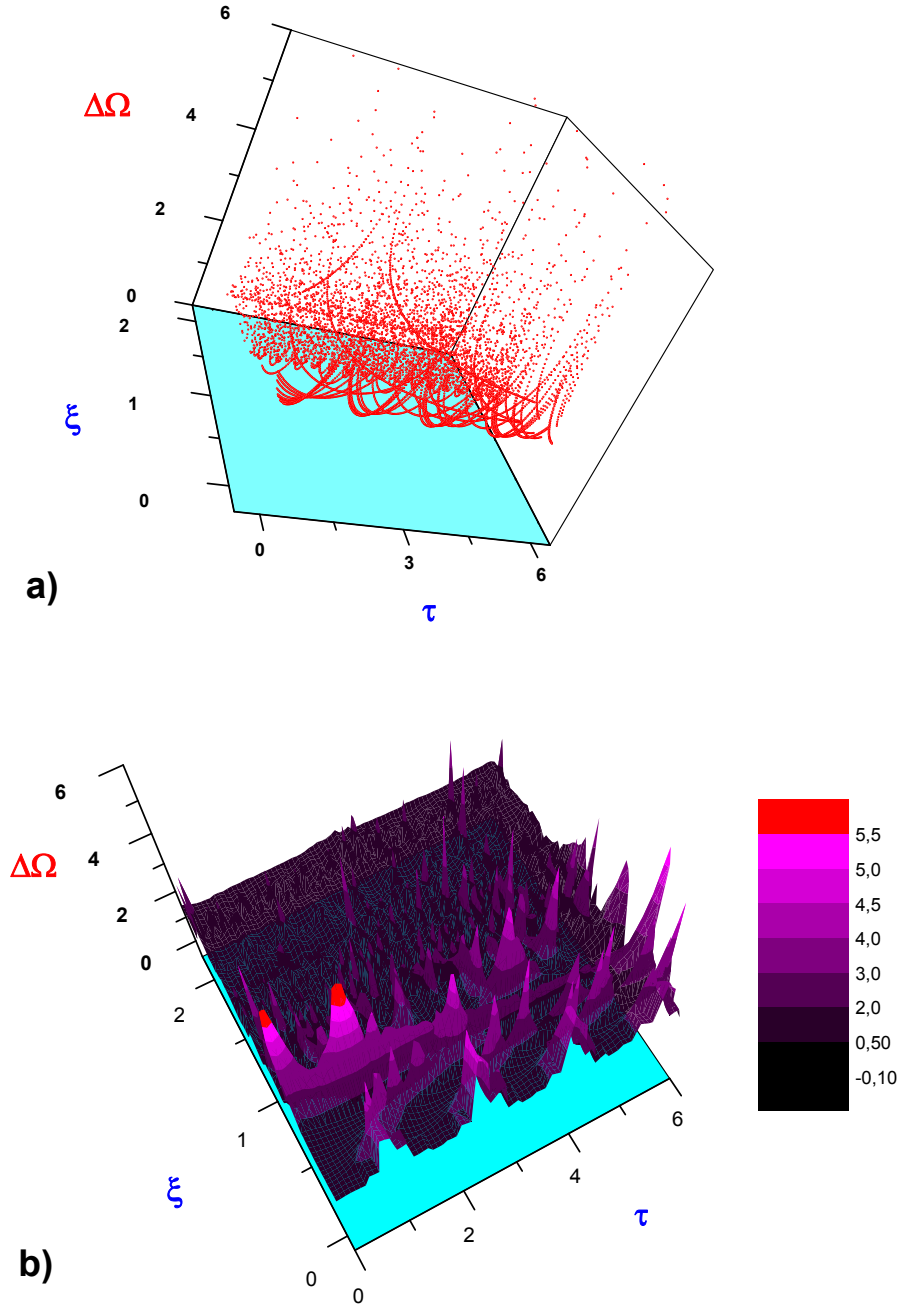

Figure 7. for $S = -1$ in Eqs. (65 and 66) shows some features of $\Delta\Omega$ propagation in the plane (ξ, τ). It is observed both in the panel (a) in the form of scattered points, and in the level surface of the panel (b) that there are patterns of intense peaks regularly spaced. It is also noted that for $\xi \approx 1$ there is a rather extensive barrier of these intense peaks around these intermediate waters.

to understand these questions better by studying the wavenumber $\kappa(h)$ and frequency $\nu(h)$ behavior as a function of depth h. In this way, it is important to notice that in this case for $S = -1$, we have that along whole intermediate water region, κ^2 is a negative number, therefore the dimensionless wave number κ is an imaginary complex number and W(see Eq. 46) is an oscillating propagating wave in this region. Furthermore, in this particular case where both $\kappa(h)$ and $\nu(h)$ are imaginary, we would like also to point out that during W propagation in intermediate waters, it reaches a strong barrier near the dimensionless intermediate depth $h \approx h_i = 1$. More specifically, in this situation we note that the phase velocity $U_{\Im}(h)$ (see Eqs. 56 and 66) have null value as the depth reaches $h = h_{c,-1}$, where the depth $h_{c,-1}$ is written as,

$$h_{c,-1} = \frac{\left(15L_5N_1 - 6L_3N_3 + 5\sqrt{15L_5{}^2N_1{}^2 - 6N_1L_3L_5N_3 + 6L_1L_5N_3{}^2}\right)N_3{}^2}{5N_1L_3L_5N_3 - 6L_3{}^2N_3{}^2 + 25L_5{}^2N_1{}^2 + 25L_1L_5N_3{}^2}$$
$$\approx 1.06\,. \tag{67}$$

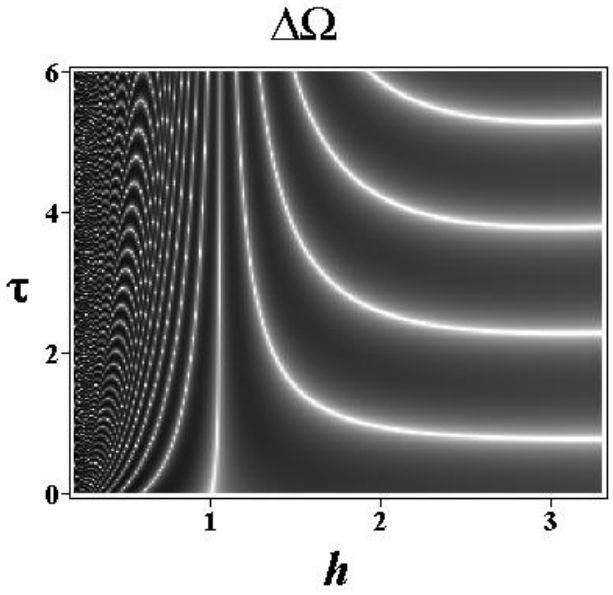

Figure 8. for the case where $S = -1$ in Eqs. (65 and 66), shows in a grayscale map the temporal evolution of $\Delta\Omega$ propagation at depths in the range $h_s \leq h \leq h_d$. Since in this figure the brightest tones represent intense amplitudes, it can be observed that around depths $h = h_{c,-1}$ (see Eq. 67) a barrier of high wave amplitudes is established, moreover it can also be observed that the pattern of these intense peaks are quite different in shallow waters from those in deeper waters.

Thus, even for the present time dependent non linear problem, the depth $h_{c,-1}$ behaves as a classical wave propagation barrier. These interesting features could be better observed in gray scale map in Fig. (8), where in this figure the waveform $\Delta\Omega$ time evolution is described as the depth h varies. Moreover we notice in this figure that in deep waters for $h \geq h_d \approx 2.11$, the waveform W(see Eq. 46) shows a discrete pattern of intense values. Such patterns delimit regions between high and low wave magnitude in accordance with wave high amplitude criterion stated in Eq. (57). More explicitly, it is also observed from Figs. (7b and 8) that for depths $h_{c,-1} \leq h \leq h_d$, holes are formed between and around the multi peaks of W. Notice that a long these troughs the intensity of W(see Eq. 46) shows very low values. On the other hand, when these waves reaching shallow waters depths $h \leq h_s$, we can yet observe in Fig. (8) the occurrence of discrete alternating patterns of high and low magnitudes of the wave W. But now, they present a self-similar structure that resembles the usual

Talbot patterns in rogue and breather waves interference phenomena (Zhang et al. 2014). Below, we continue to analyze another interesting feature of these non linear waves propagating in intermediate waters, more specifically we will study the case where the wave propagation initial condition try to represent a possible wave crest.

Case S = 11

In this way, adopting $S = 11$ as an initial value for wave strength in Eqs. (65 and 66) and using the Table(II) data, we observe that in very deep waters ($h \gg h_d$) the dimensionless wavenumber κ is imaginary ($\kappa^2 \leq 0$) and W(see Eq. 46) is an oscillating wave in these regions. In addition, we also notice that at the depth $h_{\kappa,11}$ the wavenumber has null value $\kappa(h_{\kappa,11})$=0. Thus, follows of Eq. (65) that $h_{\kappa,11}$ should satisfies:

$$\begin{aligned} h_{\kappa,11} &= \frac{22{N_3}^2}{5L_5N_1 - 2L_3N_3} \\ &\approx 2.23. \end{aligned} \tag{68}$$

On the other hand, Eq. (65) shows that $\kappa(h) > 0$ for depths such that $h < h_{\kappa,11}$, so in this situation the wave should be evanescent. This fact resembles the wave tunneling effect and in this particular case, the depth $h_{\kappa,11} \approx h_d$ behaves as a turning point in potentials or penetrable barriers in Quantum Mechanics (Schiff 1955). In addition, in this particular case where $S = 11$, Eqs. (55 and 66) show that regions between deep and intermediate waters the phase velocity $U_{\Re}(h)$ reaches a null value at $h = h_{c,11}$, being $h_{c,11}$ given by:

$$\begin{aligned} h_{c,11} &= \frac{\left(66L_3N_3 - 165L_5N_1 + 55\sqrt{15{L_5}^2{N_1}^2 - 6N_1L_3L_5N_3 + 6L_1L_5{N_3}^2}\right){N_3}^2}{5N_1L_3L_5N_3 - 6{L_3}^2{N_3}^2 + 25{L_5}^2{N_1}^2 + 25L_1L_5{N_3}^2} \\ &\approx 1.02 \end{aligned} \tag{69}$$

These results are best visualized in Fig. (9), where a grayscale map for the $\Delta\Omega$ amplitudes is shown. In the Fig. (9) we observe that in ultra-deep waters ($h \gg h_d$), the waveform $\Delta\Omega$ is oscillatory and presents a well defined almost periodic pattern of large intensity values (see Eq. 57). However, for depths in the boundary between deep waters where $h_d \approx h_{\kappa,11}$, Fig. (9) shows that occurs a barrier that inhibits the existence of intense propagating waves at depths $h < h_{\kappa,11} \approx 2.2$, so that in these regions the wave becomes evanescent and starts to propagate as a hole soliton like. In addition, Fig. (9) also shows that the propagation of this evanescent wave in typically intermediate waters encounters an impenetrable barrier at $h \approx h_{c,11} \approx 1$ (see Eq. 69), which forbids the propagation of these hole solitons in typical intermediate and shallow waters regions. In the next section we will summarize our main results.

CONCLUSIONS

In this article we theoretically proposed that waves similar to solitons (see Eq. 46) can propagate in intermediate waters. More specifically, we notice that for harmonic waves with period T propagating in an ocean with depth d, we characterize the intermediate water scale at the depths around $d \approx d_i$

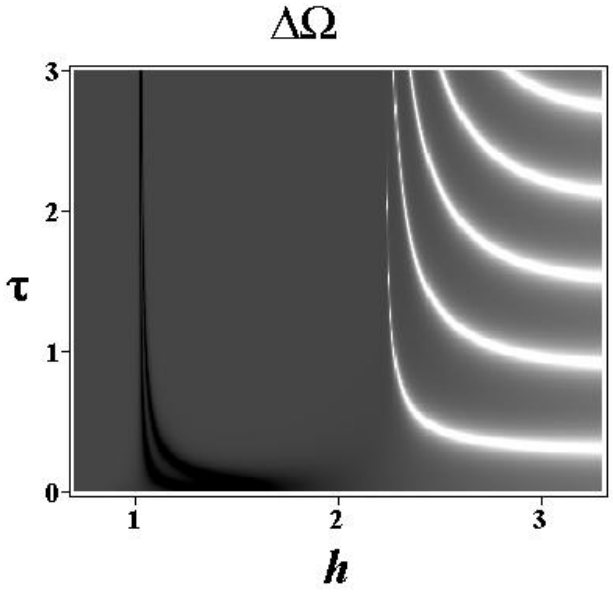

Figure 9. for $S = 11$ in Eqs. (65 and 66), shows in a gray scale map the behavior of the $\Delta\Omega$ temporal evolution as a function of h. In this map the brightest tones represent the greatest amplitude values of the wave. It is noted that a barrier for these oscillating waves with high amplitudes occurs at depth $h = h_{\kappa,11}$ (see Eq. 68), and that after evanescently crosses this barrier, the wave becomes a hole soliton like. Moreover, this hole soliton reaches another barrier at $h = h_{c,11}$ (see Eq. 69) which forbids its propagation in shallow water.

such that $c_0(T, d_i) \approx c_\infty(T)$ (see Eqs. 10 and 12), as well as we shown that d_i *is the depth where the wave group velocity u reaches a maximum value* u_{max} (see Eq. 18 and Fig. 2b). In this context, instead of we studied some wave propagation features in the wavelength $\lambda(T, d)$–domain, based on the Snell's law for wave refraction, here we analyze the behavior of the angle of refraction $\theta(h)$ as the dimensionless depth $h = d/d_i$ varies (compare Figs. 1 and 2). In this way, it was possible to analyze the wave propagation features only in the $\theta(h)$-domain. In other words, this more geometrical procedure allowed us to rewrite the dispersion relationship (1) as the transcendental Eq. (15) and numerically solve it (see Appendix A for details) for depths h in intermediate water restricted to the interval $h_s < h < h_d$ (see Fig. 3 and Table I). In addition, for waves propagating in this particular depth range and adopting a *suitable reference frame* that horizontally moves with the mean velocity $\Delta\upsilon$ (see Eq. 23) related to *the particles that are located between the wave crest and the wave trough*, we expand the dispersion relationship (32) of these waves in a Chebyshev polynomial base (see Fig. 4, Eqs. 33 and 34). In this way, this last procedure permitted us to apply the semi-classical connection between frequency $\rightarrow$ temporal derivative and wavenumber $\rightarrow$ spatial derivative (see Eqs. 42 and 41) and made it feasible to derive a new nonlinear wave equation (see Eq. 43) similar to the KdV equation, where one of its possible solutions is just the waveform W (see Eq. 46). In addition, we shown that the behavior of the W waveform *is strongly dependent on the initial conditions* imposed on the propagation of such waves. For instance, if in intermediate waters W is constrained to propagates with the phase velocity equal to the wave group velocity $u(h)$ of a single harmonic wave train, it can be seen from Figs. (5 and 6) that in this case, W evolves from a high trough in deep water to a thin hole soliton in shallow water. Another particular situation studied in this work concerns taking, as an initial condition, the value of the waveform dimensionless strength S in distant past times (see Eq. 62). More specifically, we analyze the values of $S = -1$ and $S = 11$. For instance, in the case where we adopted $S = -1$, we see from Fig. (7) that in some regions along the whole range of intermediate waters, the amplitude of the waveform W can reach very high multi peaks values (see Eq. 57). Besides, notice that such discrete

patterns of intense fields in shallow waters is quite distinct from those occurring in deep waters (see Fig. 8).

Also in this case where $S = -1$, we see that intermediate waters near the depth $h \approx h_{C,-1} \approx 1$ present a barrier formed by waves with high amplitudes (see Eq. 67 and Fig. 8). Another particular situation analyzed in this work, concerns taking $S = 11$ in Eqs. (65 and 66). In this last case, the waveform W in deep waters propagates as an oscillating wave and presents high intensity multi peaks values in this region, however when penetrating in depths around $h \approx h_{\kappa,11} \approx 2.2$, the waveform W encounters a barrier (see Eq. 68 and Fig. 9) and after crossing this barrier and penetrating in intermediate waters, W behaves an evanescent wave (see Fig. 9). Besides, in this region these waves are very similar to a hole soliton, that during their propagation encounter another barrier in depths close to $h \approx h_{C,11} \approx 1$ (see Eq. 69 and Fig. 9). However, this last barrier makes it impossible for W to reach shallow waters (see Fig. 9). In addition, in both cases for $S = -1$ and $S = 11$, it is also important to notice that these waves are quite refractive, since their phase velocity varies strongly with depth h in such situations (see Eqs. 55 and 56) .

Finally, it is important to point out that some of these theoretical results presented here are introductory, and in future works other features about the propagation of these particular non linear ocean waves should be addressed as well. To this end, more specifically we are studying the role of uniform currents in the propagation of these nonlinear waves in intermediate waters, as well as we are generalizing the initial conditions for this problem, so that S (with $\Re[S] \neq 0$ and $\Im[S] \neq 0$) can admit general complex values in Eq. (64) and if this procedure allows us to introduce some physical mechanisms related to the dissipation of wave energy. Efforts on these issues are in progress and planned to be submitted for publication as soon as possible.

Acknowledgments

The author would like to express his deep gratitude to Prof. Carlos Eduardo Parente Ribeiro for his insightful lectures about the ocean research, without these clear and seminal discussions, it would be impossible to carry out this work.

REFERENCES

ARFKEN GB & WEBER HJ. 1999. Mathematical methods for physicists. American Association of Physics Teachers.

BABANIN A. 2011. Breaking and dissipation of ocean surface waves. Cambridge University Press.

BREMNES JB. 2019. Ensemble Postprocessing Using Quantile Function Regression Based on Neural Networks and Bernstein Polynomials. Month Weat Rev 148(1): 403-414. doi:10.1175/MWR-D-19-0227.1.

CAMPOS RM, ALVES JHGM, SOARES CG, GUIMARAES LG & PARENTE CE. 2018. Extreme wind-wave modeling and analysis in the south Atlantic ocean. Ocean Modelling 124: 75-93. doi:10.1016/j.ocemod.2018.02.002.

CAMPOS RM, SOARES CG, ALVES JHGM, PARENTE CE & GUIMARAES LG. 2019. Regional long-term extreme wave analysis using hindcast data from the South Atlantic Ocean. Ocean Eng 179: 202-212. doi:10.1016/j.oceaneng.2019.03.023.

CHABCHOUB A, HOFFMANN NP & AKHMEDIEV N. 2012. Observation of rogue wave holes in a water wave tank. Journal of Geophysical Research: Oceans 117(C11). doi:10.1029/2011JC007636.

CHABCHOUB A, KIMMOUN O, BRANGER H, KHARIF C, HOFFMANN N, ONORATO M & AKHMEDIEV N. 2014. Gray solitons on the surface of water. Phys Rev E 89: 011002. doi:10.1103/PhysRevE.89.011002.

DEAN RG & DALRYMPLE RA. 1991. Water Wave Mechanics for Engineers and Scientists. Advanced series on ocean engineering. World Scientific.

DINGEMANS MW. 1997. Water Wave Propagation Over Uneven Bottoms. Advanced series on ocean engineering. World Scientific Pub.

DRAZIN PG & JOHNSON RS. 1989. Solitons: an introduction. Cambridge Texts in Applied Mathematics. Cambridge University Press.

HOLTHUIJSEN LH. 2010. Waves in Oceanic and Coastal Waters. Cambridge University Press.

JAWAD AJM. 2013. Soliton solutions for the Boussinesq equations. J Math Comput Sci 3(1): 254-265.

JOGESH BABU G, CANTY AJ & CHAUBEY YP. 2002. Application of Bernstein polynomials for smooth estimation of a distribution and density function. J Stat Plan Infer 105(2): 377-392. doi:10.1016/S0378-3758(01)00265-8.

KAKIZAWA Y. 2004. Bernstein polynomial probability density estimation. J Nonparam Stat 16(5): 709-729. doi:10.1080/10485250420001914 86.

KHARIF C, PELINOVSKY E & SLUNYAEV A. 2008. Rogue waves in the ocean. Springer Science & Business Media.

KIBLER B, CHABCHOUB A, GELASH A, AKHMEDIEV N & ZAKHAROV VE. 2015. Superregular Breathers in Optics and Hydrodynamics: Omnipresent Modulation Instability beyond Simple Periodicity. Phys Rev X 5: 041026. doi:10.1103/PhysRevX.5.041026.

LIGHTHILL MJ. 1978. Waves in Fluids. Cambridge University Press.

MILEWSKI PA. 2005. Three-dimensional localized solitary gravity-capillary waves. Communications in Mathematical Sciences 3(1): 89-99.

MILEWSKI PA & KELLER JB. 1996. Three-Dimensional Water Waves. Studies in Applied Mathematics 97(2): 149-166. doi:10.1002/sapm1996972149.

OSBORNE AR. 2010. Nonlinear Ocean Waves and the Inverse Scattering Transform. ISSN. Elsevier Science.

PRESS W, TEUKOLSKY S, VETTERLING W & FLANNERY B. 2007. Numerical Recipes 3rd Edition: The Art of Scientific Computing. Cambridge University Press.

REMOISSENET M. 1999. Waves Called Solitons: Concepts and Experiments. Advanced Texts in Physics. Springer.

SCHIFF LI. 1955. Quantum Mechanics. International series in pure and applied physics. McGraw-Hill.

SVENDSEN IA. 2006. Introduction to Nearshore Hydrodynamics. Advanced series on ocean engineering. World Scientific.

YANG J. 2010. Nonlinear waves in integrable and nonintegrable systems. SIAM.

ZHANG Y, BELIĆ MR, ZHENG H, CHEN H, LI C, SONG J & ZHANG Y. 2014. Nonlinear Talbot effect of rogue waves. Phys Rev E 89: 032902. doi:10.1103/PhysRevE.89.032902.

How to cite

GUIMARÃES LG. 2022. Some features of solitonic waves propagating in intermediate waters. An Acad Bras Cienc 94: e20210678. DOI 10.1590/0001-3765202220210678.

Manuscript received on May 5, 2021;
accepted for publication on December 13, 2021

LUIZ GALLISA GUIMARÃES
https://orcid.org/0000-0001-5699-1251

Universidade Federal do Rio de Janeiro-UFRJ, Programa de Engenharia Oceânica-COPPE, Centro de Tecnologia da UFRJ, Av. Athos da Silveira Ramos, Cidade Universitária, 21941-611 Rio de Janeiro, RJ, Brazil

E-mail: LuLa@if.ufrj.br; LGG@oceanica.ufrj.br

APPENDIX A - AN ALTERNATIVE ALGORITHM FOR $\theta(H)$ AND $\lambda(T,\theta)$ NUMERICAL CALCULATIONS

Many of the numerical results shown in this work depend on having previously calculated the wavelength λ. On the other hand, in the case of harmonic waves with period T propagating in oceans with finite depth d, the literature (Dean & Dalrymple 1991, Lighthill 1978) shows that for calculate $\lambda(T,d)$ it is necessary to solve numerically the transcendental Eq. (5). To perform this numerical task for a given period T and depth d, very accurate algorithms and approximate formulas were developed (Dean & Dalrymple 1991, Holthuijsen 2010, Svendsen 2006). However in the present work we adopt a more geometrical picture, where for a given dimensionless depth h (see Eq. 12) our procedure consists of previously solving the *single parameter* transcendental equation (15) for the refraction angle $\theta(h)$, so that later using the Snell's law (see Eq. 14) we can then calculate the wavelength $\lambda(T,d)$. In other words, we will see below, that this algebraic procedure allows us to obtain *a general result*, that makes graphically explicit *all the possible real solutions* of the transcendental equation (15) for $\theta(h)$. In addition, we will also observe (see the Fig. (A1) below) that these numerical solutions for $\theta(h)$ (or $\sin\theta$) *do not explicitly depend on the period* T. We will discuss these results in more detail below. More specifically, in order to develop this numerical procedure, first it is suitable to rewrite Eq. (15) as follows:

$$s_{n+1} = 1 - \frac{2}{1+\exp(2\,h\,/\,s_n)}\;;\; n = 0, 1 \ldots n_{prec}\,. \tag{70}$$

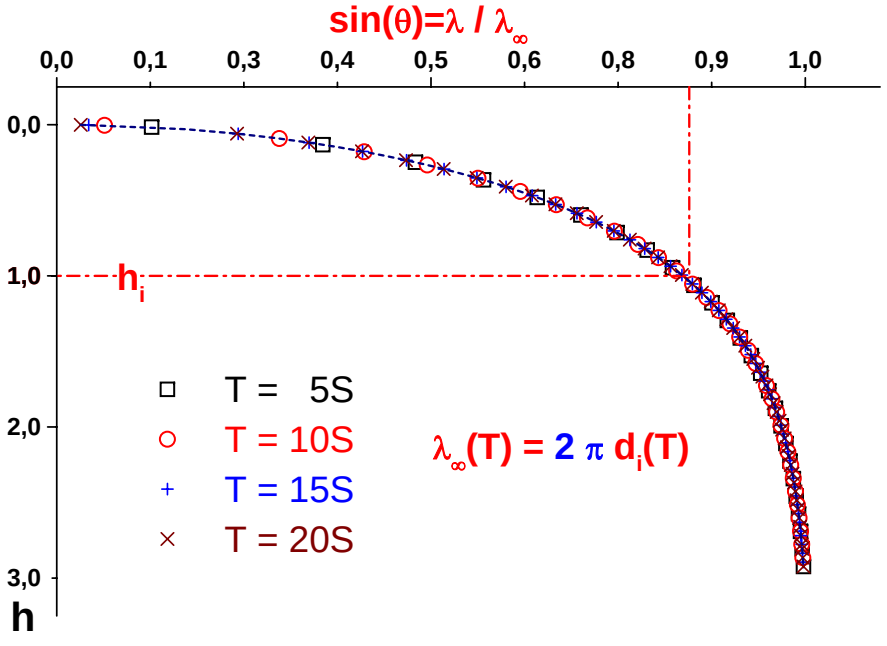

Figure A1. Shows for some wave periods T the behavior of $\sin\theta(h)$ as a function of the normalized depth h. For an accuracy of 10^{-6}, the values of $\sin(\theta)$ were calculated using the algorithm(70) to solve numerically Eq. (15). Notice that the wavelength $\lambda(T,d)$ satisfies the Snell's law(14), $\lambda = \lambda_\infty \sin(\theta)$.

Such that, for a given dimensionless depth h we can iteratively apply Newton's method in the difference equation (70). Where in this Eq. (70) the parameter s_n represents the n-th estimate for $\sin(\theta_n)$ value, and n_{prec} is the maximum number of iterations used for a specific required precision. However, this numerical procedure is sensitive to the initial guess value. Moreover, for waves propagating in intermediate waters such that $\forall h,\ h_s \leq h \leq h_d$, using a suitable Padé rational

approximation (Press et al. 2007) to rewrite Eq. (15), it was possible to derive the following estimate for solutions of Eq. (15),

$$\sin(\theta) \approx \frac{h}{\sqrt{3.682 - 9.894\,h + \sqrt{97.90 - 52.95\,h + 13.56\,h^2}}} \quad . \tag{71}$$

Besides, it was verified numerically stable to use Eq. (71) as an initial guess for implement the algorithm(70) $\forall h,\ h_s \leq h \leq h_d$. For instance (see Eqs. 18 and 19), for an accuracy around 10^{-6}, taking $h = h_i = 1$ in above Eq. (71) and using such numerical result as initial guess in Eq. (70), we obtained after $n_{prec} = 37$ iterations the following estimate for

$$\sin(\theta_m) \approx 0.83356. \tag{72}$$

In addition, using the same precision criteria of 10^{-6}, we verified the accuracy and stability of the above algorithm for other values of the wave period T in the interval $5s \leq T \leq 20s$, and depths range beyond the intermediate waters such that $0.1 \leq h \leq 3$. These results are summarized in Fig. (A1) and for all of them, the method reaches a satisfactory convergence after a maximum number of iterations $n_{prec} < 100$.